

Tropical variability and stratospheric equatorial waves in the IPSLCM5 model

Pauline Maury · François Lott · Lionel Guez · Jean-Philippe Duvel

Received: 21 September 2011 / Accepted: 12 December 2011 / Published online: 31 December 2011
© Springer-Verlag 2011

Abstract The atmospheric variability in the equatorial regions is analysed in the Earth System Model pre-industrial simulation done at IPSL in the framework of CMIP5. We find that the model has an interannual variability of about the right amplitude and temporal scale, when compared to the El-Niño Southern Oscillation (ENSO), but that is too confined to the western Pacific. At the intra-seasonal periods, the model variability lacks of large-scale organisation, and only produces one characteristic Madden-Julian Oscillation every 10 winters typically. At shorter time-scales and in the troposphere, the model has Rossby and Kelvin Convectively Coupled Equatorial Waves (CCEWs), but underestimates the Kelvin CCEWs signal on OLR. In the model stratosphere, a composite analysis shows that the Temperature and velocities fluctuations due to the Kelvin waves are quite realistic. In the model nevertheless, the stratospheric waves are less related to the convection than in the observations, suggesting that their forcing by the midlatitudes plays a larger role. Still in the model, the Kelvin waves are not predominantly occurring during the life cycle of the tropospheric Kelvin CCEWs, a behaviour that we find to be dominant in the observations. The composite analysis is also used to illustrate how the waves modify the zonal mean-flow, and to show that the model Kelvin waves are too weak in this respect. This illustrates

how a model can have a reasonable Kelvin waves signal on the velocities and temperature, but can at the same time underestimate their amplitude to modify the mean flow. We also use this very long simulation to establish that in the model, the stratospheric equatorial waves are significantly affected by ENSO, hence supporting the idea that the ENSO can have an influence on the Quasi-Biennial Oscillation.

Keywords Tropical variability · El Niño Southern oscillation · Intra-Seasonal oscillations · Quasi Biennial oscillation · Stratospheric equatorial waves · Convectively coupled equatorial waves · Stratosphere

1 Introduction

The fact that the mean state and the variability of the stratosphere affect the tropospheric climate is now well established. This is in part due to radiative and chemical effects, essentially related to the stratospheric ozone that absorbs the solar UV, and to the stratospheric water vapour that has a significant greenhouse effect (Salomon et al. 2010). This influence of the stratosphere is also related to dynamical effects, some specific modes of the stratospheric variability propagating downward in the stratosphere, like the Quasi-Biennial Oscillation (QBO) (Baldwin et al. 2001) in the tropics, and the Arctic Oscillation (AO, Baldwin and Dunkerton 2001) in the mid latitudes. These modes of stratospheric variability significantly influence the surface climate in various regions, at least in the mid-latitudes (for the QBO see Holton and Tan 1980; Anstey et al. 2010; for the AO see Baldwin and Dunkerton 1999; Christiansen 2001; Douville 2009; Lott et al. 2005; Nikulin and Lott 2010).

This paper is a contribution to the special issue on the IPSL and CNRM global climate and Earth System Models, both developed in France and contributing to the 5th coupled model intercomparison project.

P. Maury · F. Lott (✉) · L. Guez · J.-P. Duvel
Institut Paul Simon Laplace (IPSL) and Laboratoire
de Météorologie Dynamique, Ecole Normale Supérieure,
24 rue Lhomond, 75235 Paris Cedex 05, France
e-mail: flott@lmd.ens.fr

Although less documented, it is also well established that the stratosphere can affect the relations between the tropical troposphere and the midlatitudes. For instance, the ENSO impact on the North Atlantic region (Fraedrich and Muller 1992), is more pronounced in atmospheric models that include a stratosphere (Cagnazzo and Manzini 2009), because the mid-latitude planetary waves fluxes into the stratosphere are stronger during ENSO (Sassi et al. 2004). One difficulty of studying this problem, is that the tropical tropospheric variability is dominated by ENSO whereas the stratospheric one is dominated by the QBO. Both have pronounced quasi-biennial signals, which are quite distinct according to Barnett (1992), so their effects can be difficult to disentangle: one can take for an ENSO effect a QBO effect and vice et versa. This is rendered even more complicated by the fact that, (1) the influence of these two tropical oscillations combine in a nonlinear way (Calvo et al. 2009) and that, (2) the ENSO and QBO interact dynamically with each other (Maruyama and Tsuneoka 1988; Taguchi 2010). A good dynamical reason for this relation can be that during ENSO the tropical upwelling driven by the midlatitude waves increases (Hardiman et al. 2007), and this can have a significant effect on the QBO period according to Dunkerton (1997). Another more direct reason, given by Taguchi (2010), is that the ENSO affects the forcing of the equatorial waves, because these waves are in good part driven by the convection (Manzini and Hamilton 1993; Ricciardulli and Garcia 2000; Horinouchi et al. 2003). Our analysis of the tropical variability from the intra-seasonal scales of ENSO to the synoptic scales of the equatorial waves will address this issue for the case of a coupled model.

Because the significance of the stratosphere is now well established, a good part of the ESMs participating to the Coupled Model Intercomparison Project no. 5 (CMIP5) represent it well. Following these groups of modellers, the atmospheric model from the Laboratoire de Météorologie Dynamique (LMDz, Hourdin et al. 2006) that enters into the IPSL ESM for CMIP5 (IPSLCM5), includes a good part of the stratosphere representation reported in Lott et al. (2005). An essential difference between models with a stratosphere is that some of them simulate a QBO, like the Met Office's (Hardiman et al. 2010) or the Max-Planck Institute's (Giorgetta et al. 2006) climate models whereas some other do not, like the IPSLCM5 (see Lott et al. 2005). The fact that a model does not simulate the QBO is in general related to: (1) its insufficient vertical resolution in the lower stratosphere, (2) to an under-representation of the equatorial waves that enter into the stratosphere, and (3) to a deficient non-orographic gravity wave drag. Of course this different causes are intimately related, with for instance a too coarse vertical resolution limiting the model ability to represent well the vertical propagation of the

resolved equatorial waves (Boville and Randell 1992). It is therefore essential to measure the realism of the equatorial waves the models can represent explicitly, like the gravest equatorial waves analysed in Lott et al. (2005).

The simulation of Equatorial waves in models has been the subject of many studies, with researchers from the tropical meteorology community identifying the CCEWs in the troposphere (Wheeler and Kiladis 1999), and those from the stratospheric community looking at the freely propagating equatorial waves that enter in the lower stratosphere (recent satellite observations are in Ern et al. 2008). A priori, this separation is not really justified since the CCEWs organize convection and since the stratospheric equatorial waves are in part forced by convection. As an illustration, the spectral analysis in Hendon and Wheeler (2008) have shown that the spectral signature of the stratospheric waves is quite close to that of the CCEWs, with the stratospheric signal slightly faster than the tropospheric one. This suggests that a good fraction of the stratospheric waves accompany the development of the CCEWs, their faster time-scale resulting from the fact that the faster disturbances have a larger vertical wavelength and are less dissipated. If predominant, this scenario should tell that the models with insufficient CCEWs would fail in simulating the right amount of stratospheric waves. To analyse these issues, the method in Lott et al. (2009) for extracting the life cycle of the waves, can be well adapted, since it has proved to be relevant for both models and reanalysis. Note nevertheless that the waves analysed in Lott et al. (2009) are those with wavenumber $s < 10$, which can be a limitation, but for which we know from satellites observations that the reanalysis datasets are quite realistic.

The purpose of the paper is twofold. The first is to document the large-scale tropospheric tropical variability in the model, from the interannual ENSO oscillations, to the intra-seasonal Madden-Julian Oscillation (MJO) oscillations, and down to the synoptic time-scales of the equatorial waves. The second purpose of the paper is to analyse the simulation of the stratospheric equatorial waves and to report their relation with the convection below. In this context we will pay a particular attention to the relation between stratospheric waves and tropospheric equatorial waves, as well as on the relation between ENSO and the stratospheric waves.

The plan of the paper is as follows. Section 2 presents a description of the model, of the observational datasets, and the diagnostics of the tropospheric tropical variability including the inter-annual and the intra-seasonal time scales. Section 3 analyses equatorial waves, their relation with convection and their sensitivity to the ENSO phase. In this section, we will focus on the Kelvin waves, and use the fact that the simulations are very long, which enable to

extract via a composite method, the effect of the waves on the large scale flow. Section 4 summarizes the results.

2 Interannual and intra-seasonal variabilities

The experiment we look at is a 1,000 years long pre-industrial simulation done with the fully coupled IPSL ESM, IPSLCM5, and where the CO₂ emission corresponds to the 1850 value. This simulation couples an atmospheric land surface model and an ocean sea-ice model, it also includes an interactive carbon cycle (more details are in Dufresne et al. 2011, this issue). This simulation (hereinafter called picontrl2) is initialised with oceanic, sea-ice, and vegetation fields issued from series of preliminary spin-up simulations which cumulated time is around 800 years. For the atmospheric part, the LMDz5A model is used (Hourdin et al. 2011a, this issue), at resolutions 1.875° in latitude, 3.75° in longitude, and with 39 levels in the vertical. This 39 levels version goes up to about 70 km, as the stratospheric 50-levels version of LMDz in Lott et al. (2005), with 15 levels above 20 km and the resolution in the low stratosphere is around 1.5 km. As convection parameterizations are affecting the tropical variability (for the equatorial waves see Horinouchi et al. 2003), it is mandatory to recall that LMDz5A uses the Emanuel (1993) scheme for deep convection and the Bony and Emanuel (2001) statistical cloud scheme. To evaluate how the model simulates the tropical variability we will often use the OLR fields, which are a well known proxy for the large-scale convection in the tropics and which can be compared to the NOAA-OLR datasets which covers now more than 30 years (Liebman and Smith 1996). Our choice for OLR is also motivated by the fact that most of the modes of variability analysed in this paper, (ENSO, MJO and the equatorial waves), have a signature on the deep tropical convection and thus on OLR (for the ENSO, see Chiodi and Harrison 2010; for the MJO Matthews 2000; for the CCEWS Wheeler and Kiladis 1999).

All the statistical results we will present are evaluated from daily series: the entire 30-years of the NOAA datasets, and sub ensembles of picontrl2 which lengths can vary between 200 years and the entire 1,000 years of the simulation. These lengths will be given in due place. We have quite systematically verified that in term of amplitude, all the results we will show, when significant are not much affected by the length of the model sample or by the periods it covers. Nevertheless, the use of longer series is necessary when the signals from the model are quite weak or rare.

2.1 OLR means, variances and teleconnections

Figure 1a shows the mean of the OLR for the winter period and for the 1,000 years of the pre-industrial simulation.

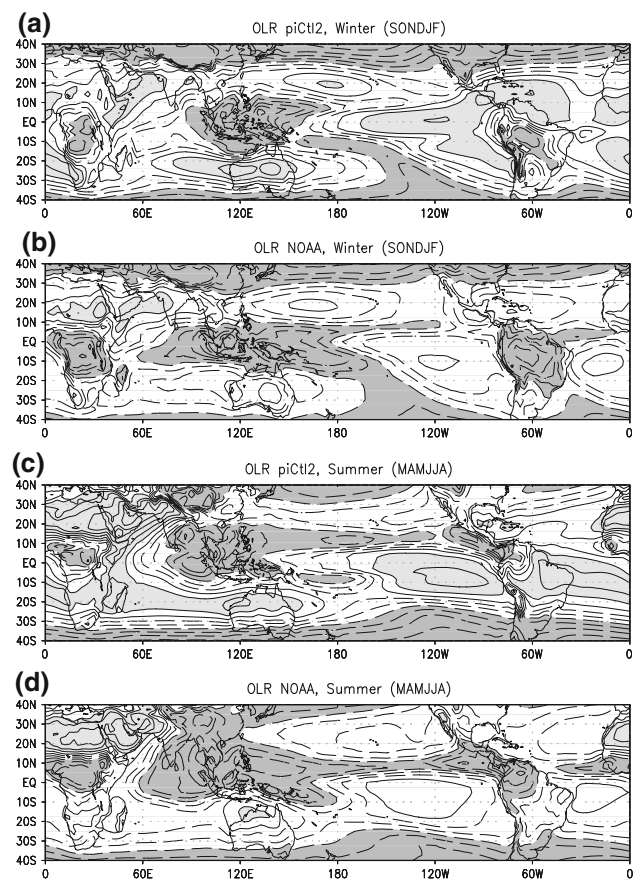


Fig. 1 Mean of outgoing longwave radiation (OLR) **a** Winter months (SONDJF) from the pre-industrial control run; **b** Same as (a) but for the NOAA-OLR; **c** Summer months (MAMJJA) from the pre-industrial control run; **d** Same as (c) but for the NOAA-OLR. CI: 10 W/m², values below 260 W/m² are dashed. Values below 240 and above 280 are lightly shaded

It shows that the model tends to produce enhanced deep convection over the maritime continent, as in the observations (Fig. 1b) but that this major centre of convective activity does not spread much over the western Pacific where the SPCZ is largely underestimated. The centre of deep convection does not extend much over the Indian ocean as well. We also see that over the subsident region of the eastern Pacific, the OLR is much larger in the model. The model also produces secondary centres of deep convection over the southern hemisphere subtropics and over Africa and South-America, but largely underestimates them. In summer (Fig. 1c, d) the model produces the expected northward shift of the convection zones. Around the longitudes of the maritime continent and India, there are now centers of deep convection over the bay of Bengal and around south-east Asia. Again, the signal does not spread enough over the Pacific ocean and in particular to the east of the Philippines archipelago. As in winter, the model locates well the regions of continental monsoonal

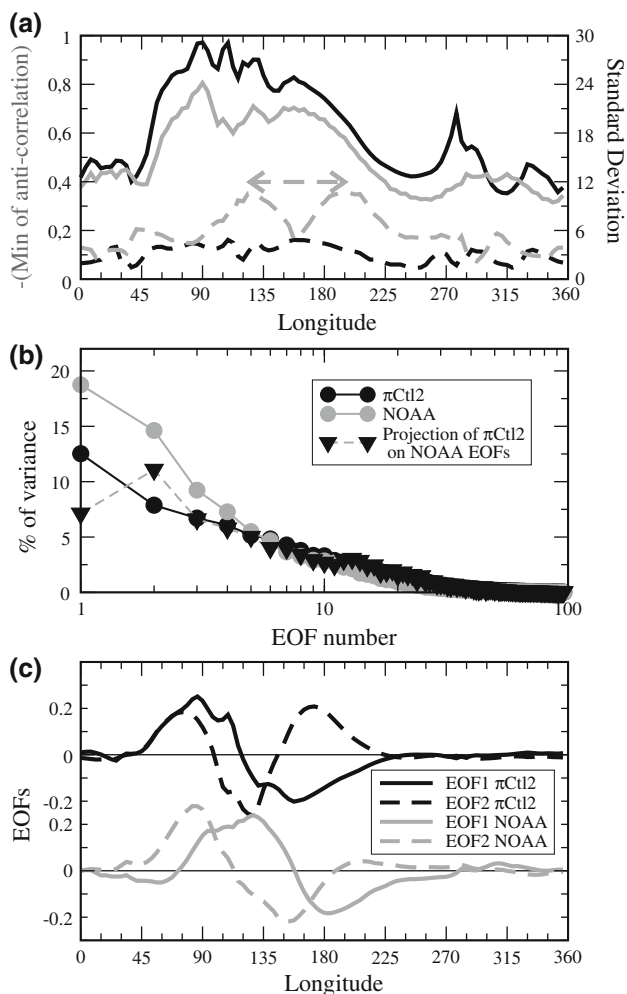


Fig. 2 Variability statistics of the OLR averaged over the Equatorial band (10°S – 10°N). *Black lines* are for the 1,000 years of picontrl2, and the *grey lines* are for the 30 years of the NOAA OLR (1979–2008). **a** Standard deviation (*solid*) and teleconnection (*dashed*). **b** EOF spectra of picontrl2, NOAA, and projection of picontrl2 on NOAA EOFs; **c** EOFs 1 (*solid*) and EOFs 2 (*dashed*) from picontrl2 (*black*) and NOAA (*grey*)

activity over the equatorial regions in Africa and South America, but underestimates their intensity.

To describe the various modes of tropical variability, we next focus on the Equatorial band by averaging the OLR signal between 10°S and 10°N . In the model (solid black curve in Fig. 2a) the OLR signal has enhanced variance over a large sector between the Indian Ocean (60°W) and the western Pacific (180°), in agreement with the observed variance (solid grey curve). Note nevertheless that the model variance almost everywhere exceeds the observed one. To evaluate the planetary-scale organisation of the convection, the dashed lines in Fig. 2a shows the maxima of anticorrelation between one point in the tropical band and any other points. If we first look at the observations (grey dashed), there is a substantial anti correlation

between the maritime continent and the central Pacific (see the grey arrow). Without ambiguity, we can associate these maxima of anti-correlation to ENSO, since they are located near the longitude of Darwin (130°) and Tahiti (210°E), places where the ENSO variability produces largely anti-correlated responses (Ropelewski and Jones 1987). The dashed black line shows that in the model, this large scale anti-correlation is in good part lost.

2.2 Modal analysis

To extract the spatial patterns that control the model variability, we next proceed to an EOF analysis of the OLR signal (still averaged between 10°S and 10°N). The EOF spectra in Fig. 2b shows that in the model the first 2 EOFs represent less than about 20% of the variance, whereas in the NOAA dataset they account for almost 35% of the variance. Beyond EOF 5, the two spectra behave quite identically. We see here that the lack of large-scale connection between geographic places in the model (grey curves in Fig. 2a) makes that the EOF spectra for the model OLR is much whiter than the corresponding spectra from the NOAA OLR (Fig. 2b). The structures of these EOFs are shown in Fig. 2c, with the first model EOF representing a seesaw for deep convection between the Indian ocean and the western Pacific, a pattern that is somehow reminiscent of the second EOF of variability from the NOAA OLR (grey dashed). The second EOF of the model again translates the much whiter structure of the model variability since it has three extrema. It corresponds to enhanced precipitation over the maritime continent and reduced convection on the two sectors immediately to the east and to the west, that is in the western and central Pacific on the one hand and over the whole Indian ocean on the other. Clearly, the lack of anti-correlation between the Maritime continent and the central Pacific in the model, makes that it has difficulties in capturing the first observed EOF, the one which is the more strongly related to ENSO (Kessler 2001).

To characterize the temporal evolution of the large-scale variability, we next follow Matthews (2000), and use the first two leading PCs. Furthermore, as the model EOFs differ significantly from the observed ones, we have verified that our results are not much changes when we project the model fields on the observed EOFs (generating pseudo-PCs). As a first illustration, the lower triangles in Fig. 2b show that the variance of the two pseudo-PCs generated this way is larger than that of the higher orders pseudo-PCs, as it is for the real PCs. Some other examples will be given.

Figure 3a, b show the spectra of the first and second PCs respectively evaluated from the first 200 years of picontrl2. In Fig. 3a we see that the PC 1 for the observations has enhanced variances at the inter-annual scale with a

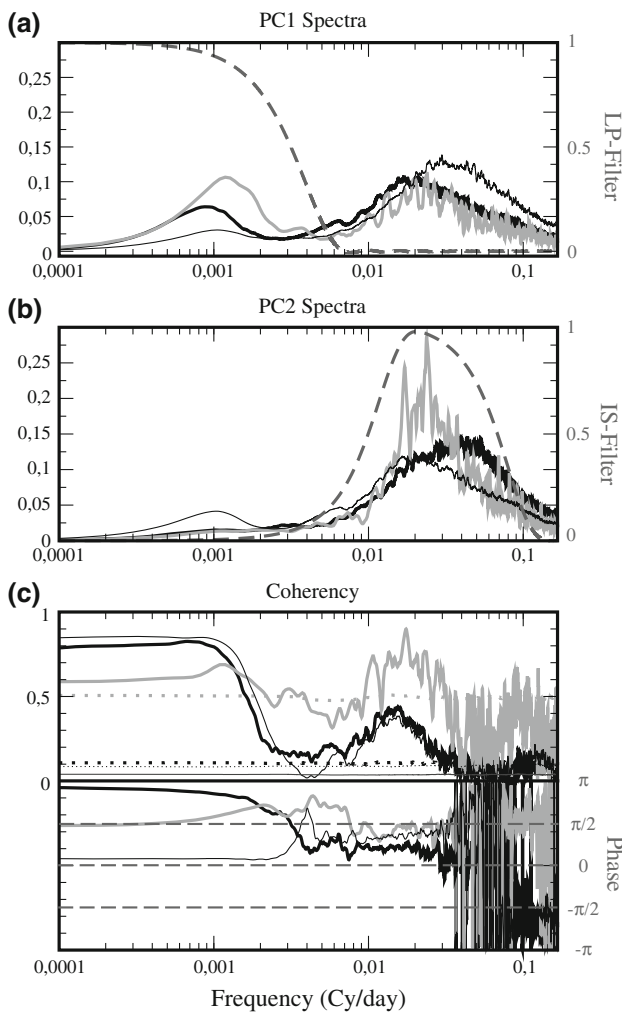


Fig. 3 Spectral analysis of the PCs 1 and 2 of the OLR. The *black lines* are from the picontrl2 simulation, the *grey curves* are from the NOAA dataset and the *thin black lines* are for the picontrl2 datas projected on the NOAA EOFs. **a** PC1s spectra and inter-annual filter used to extract the ENSO (*thick grey dashed*). **b** PC2s spectra and intra-seasonal filter used to extract the MJO (*thick grey dashed*). **c** coherency between PC1 and PC2. For the model, the spectra and co-spectra are evaluated in three steps: (1) the first 200 years in each PCs is extracted and averaged over 3 days, (2) Fourier transforms of the 2 resulting series are done, (3) the resulting periodograms and cross periodogram are smoothed by a 33% cosine window of width 3 cy/year yielding a resolution of 3.10^{-3} cy/day. In **c** the *dotted lines* are for the mean and the 1% levels, they are estimated from a monte-carlo test (see Lott et al. (2004) for details). For the NOAA dataset, the same technique is used but over the 30 years available

broad maximum around 3 years. It also has enhanced variability at the intra-seasonal scales [10–100 day]. As the EOF 1 from the observations projects well on the ENSO, we can attribute the intra-seasonal variability on the PC 1 to the ENSO signal. This attribution is supported by the fact that the PC 2 spectra in the observed OLR is almost devoid of inter-annual variations (grey curve in Fig. 3b) but has enhanced variability at the intra-seasonal periods. The behaviour of PC 1 and PC 2 from the model

have some resemblance with the observed ones, with substantial inter-annual variability in PC 1 and substantial intra-seasonal variability in both PC-1 and PC2 (thick black curves in Fig. 3a, b). The thin lines on Fig. 3a, b, are for the model “pseudo”-PCs spectra, showing that they present about the same amount of variance at the intra-seasonal and interannual periods than the real PCs, indicating again that they could be used to characterize the model variability.

To characterize the propagative aspects of the variability, Fig. 3c shows the spectral coherency between PC 1 and PC 2. In the model (thick black line in Fig. 3c) the two PCs have enhanced coherency at the intra-seasonal periods (25–100 day). Although largely significant since our temporal series are very long (200 years here) this enhanced coherency is less pronounced than the corresponding one from the NOAA OLR (grey line in the top panel). We will see in the next subsection that this weaker intra-seasonal coherency in the model, is related to the fact that the large scale OLR anomalies do not propagate eastward as regularly as in reality. A first indication that this is indeed the case is given by the phases shown in Fig. 3c. For the model the two signals in the 25–100 day band are between being in phase and being in quadrature whereas in the observations the two PCs are well in quadrature.

2.3 Composite maps

The temporal evolution of the leading PCs from the model and from the observations are shown in Fig. 4. For each PCs we also isolate its inter annual variability by using a non recursive low-pass filter that uses Kaiser windows adjusted to minimize Gibbs effects and with half power

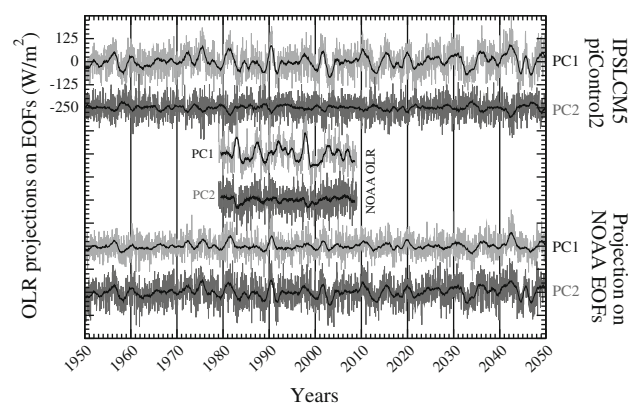


Fig. 4 Temporal evolution of the PCs of the OLR averaged over the Equatorial band. For clarity, each curves are shifted vertically and the PCs from the control run are shown over 100 years only. To characterize the inter-annual variability, the *thick black lines* represent the corresponding series after application of the low pass filter that smoothed out the inter-annual variability (see the *dashed grey curve* in Fig. 3a)

point at 1 year (see the thick grey curve in Fig. 3a and Hamming 1983; Lott et al. 2004). For the observed series, PC1 presents substantially larger inter-annual variability than PC2 and the major peaks in PC1 occur during well known ENSO-years (1982–1983 and 1997–1998 for instance). For the model, PC1 and its filtered component (1st curves on the top of Fig. 4) shows similar properties, with substantial interannual. The last 2 curves in Fig. 4 are for the model pseudo-PCs: the first one has interannual extrema at the same time as that of the “true” model PC1, which means that the true PC1 or the pseudo PC1 can as well be used.

The maps in Fig. 5a shows the OLR difference maps between positive and negative ENSO phases. These composites are built from unfiltered OLR maps from which the annual cycle has been removed, and the positive and negative ENSO phases are selected from thresholds on the filtered PC1s signals (see Fig. 5 caption for details). The model ENSO is characterised by a negative OLR signal covering the equatorial regions between 140°E and 120°W. It is also characterized by positive OLR anomalies over most of the equatorial Indian ocean. Compared to observations in Fig. 5b, the model ENSO is about the right amplitude but is substantially shifted to the west. As noticed in Leloup et al. (2008), this is a quite common defect of coupled models, with the IPSLCM5 model here behaving almost as its previous version (Marti et al. 2005).

To extract the intra-seasonal oscillations we next apply to the PC1 and PC2 series a band-pass filter with half

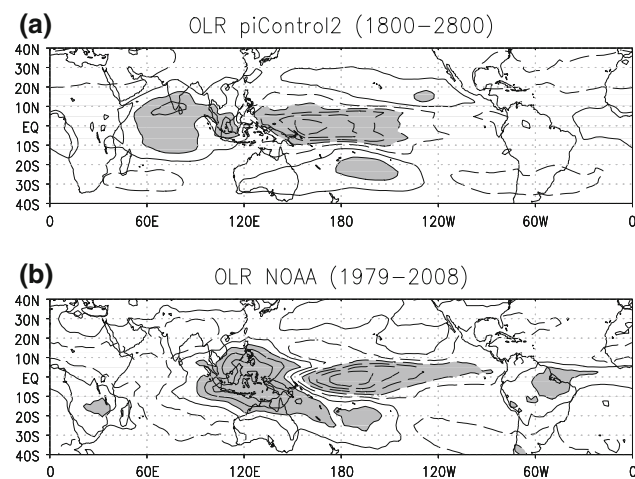


Fig. 5 OLR differences according to positive and negative ENSO phase (a) and (b) are for the difference in mean OLR for picontrol2 and NOAA respectively. $CI = 10 \text{ Wm}^{-2}$, values below -15 Wm^{-2} and above 15 Wm^{-2} are *lightly dashed*. A given date is considered as being in an positive (negative) ENSO phase, when the value of the interannual PC 1 (that is the first and third *black solid thick curves* in Fig. 4) is larger (smaller) than a given positive (negative) threshold. For both the model and the NOAA datas, the positive and negative thresholds are chosen so that 30% of dates are in positive or in negative ENSO phase (approximately 15% in each)

power points at 25 and 100 day respectively. Again this band pass filter is designed by combining two low pass filters of the type used in Lott et al. (2004), its transfer function is displayed in Fig. 3b. The filtered PC1 and 2 are then used to construct a vector, and we next evaluate the variability it represents by averaging over time its squared amplitude. Then, when this vector amplitude exceeds 1.1 times its standard deviation during more then 30 days, we consider that the selected period contains a canonical MJO. During this period we attribute each dates to a given phase dividing the filtered PC 1 and PC 2 phase space into 8 sectors (see for instance Fig. 7 in Wheeler and Hendon 2004). The result for the composite from the NOAA dataset are shown on the right column of Fig. 6, illustrating that we have captured well the MJO (see for instance Matthew 2000). For the model in the left column of Fig. 6, there is a broad agreement, indicating that the model is able to produce some MJO-type oscillations. However, the composite from the model are built using less than 100 events out of 1,000 years, whereas those from the NOAA OLR data are built using 14 events out of 30 years (consistent with the idea that there is one strong canonical Madden-Julian oscillation every 1 or 2 years typically, Goulet and Duvel, 2000). Of course these numbers are somehow arbitrary, and change when the various threshold on the amplitude and duration change. We have nevertheless verified that the 1–5 ratio between the number of MJOs in the model and in the observation stay almost unchanged. From this analysis, and in agreement with Xavier et al. (2010) we find that the coupled model simulate too few intra-seasonal oscillations, but is able to produce some.

3 Equatorial waves

3.1 Spectral analysis

To analyse the spectral signature of the equatorial waves and their relations with large-scale convection, we will follow Wheeler and Kiladis (1999) and Hendon and Wheeler (2008) among others, and make space-time spectra of the tropical signals. We will display the spectra using energy conserving pictures with log-axis and present spectral coherencies between the dynamical fields and the OLR fields. As shown by Hendon and Wheeler (2008) both the representation of the spectra in these logarithmic axis and the representation of the coherencies permit to characterise the spectral signature of the tropospheric equatorial waves, without requiring to normalize the spectra by red-noise backgrounds. In the following of this subsection, the spectra from the model are evaluated over the first 200 years of picontrol2 and compared to the spectra from the observations over the period 1979–2008.

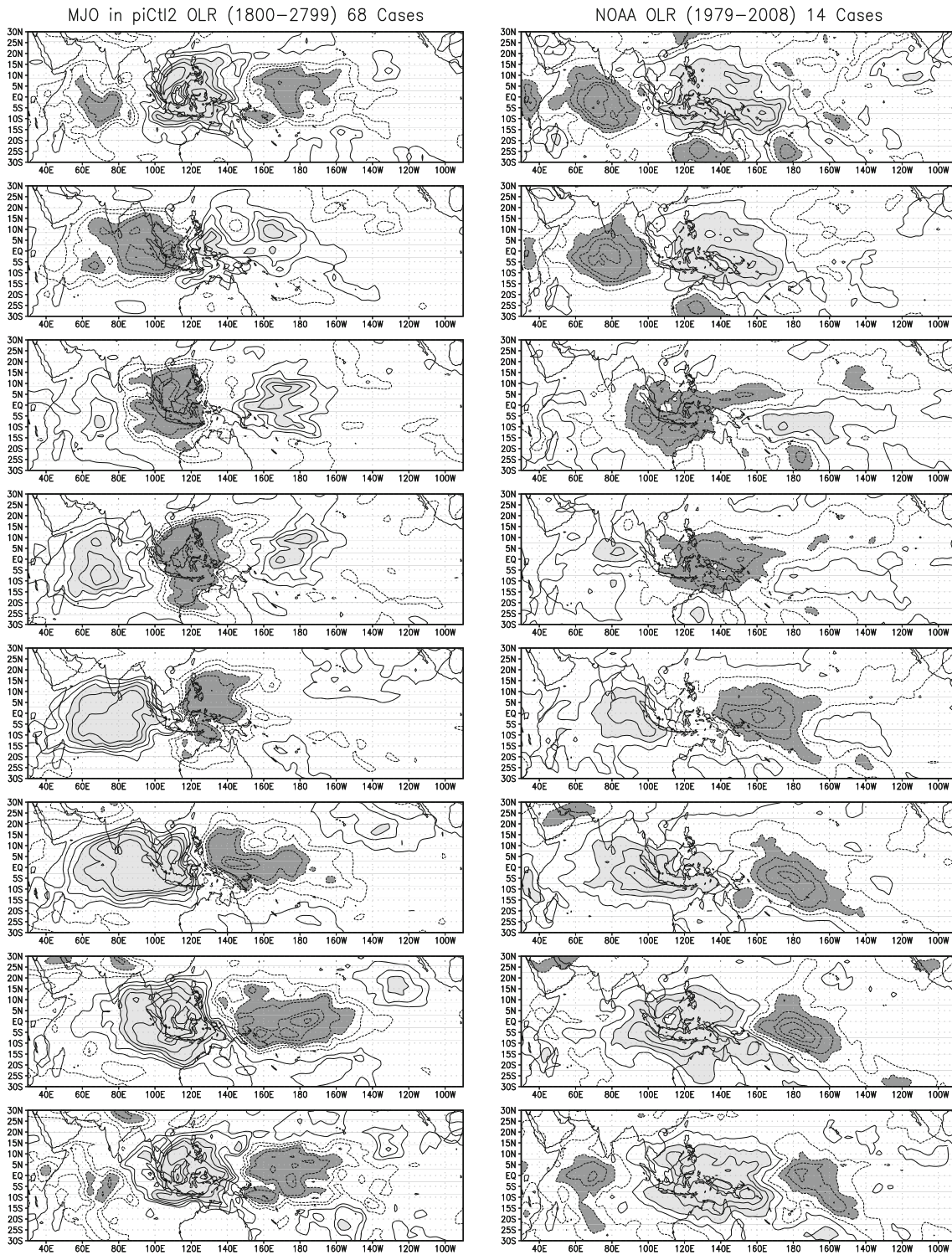


Fig. 6 Composite of OLR according to the 8 different phase of the MJO (from *top to bottom*): picontrol2 (*left*) and NOAA (*right*). CI: 10 W/m^2 , values below -15 W/m^2 and above 15 W/m^2 are lightly shaded. After filtering the PCs 1 and 2 by the interannual filter shown

in Fig. 3b, an MJO is selected when the norm of the vector forms with the filtered PCs exceed a given threshold during more than 30 days (see text for more details)

3.1.1 OLR spectra and coherency with 850 hPa zonal wind

Figures 7a and 8a show the spectra of the OLR averaged over the equatorial band from the model and from the NOAA dataset respectively. On these two figures are also presented the coherency with the zonal wind at 850 hPa averaged over the equatorial band. The y-axis for the frequency is in log-scale so the figure presents the frequency

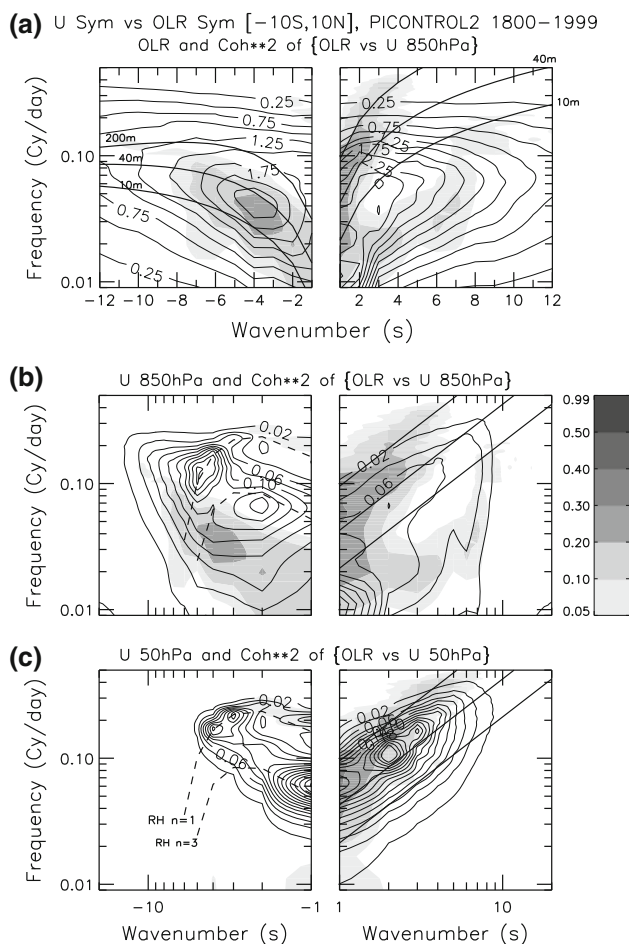


Fig. 7 Spectral analysis of OLR and zonal winds averaged over the equatorial band, picontr02 simulation for the period 1800–2000. The spectra are built from the double Fourier transform of each field averaged over the Equatorial band and for each year. From this are built periodograms and cross periodograms which are averaged over the 200 years of the datasets. The resulting estimate of the spectra and cross-spectra are further reduced by applying 30 times a 1-2-1 average in the time domain. From the impulse response to this filter we can estimate that it smoothes over around 15 points, yielding a spectral resolution of around 4.10^{-2} cy/d and increasing the number of doF to 3,000: for this value the 10, 5, and 1% level for the coherencies are at around 0.007, 0.013, and 0.06. The dispersion curves shown in *solid* are for the Kelvin and Rossby ($n = 1$) waves, with equivalent depth $h = 10, 40, 200$ m. The dispersion curves shown in *dashed* are for the Rossby-Haurwitz waves with $n = 1$ and 3, doppler shifted by a zonal wind $u = 15$ m/s

U Sym vs OLR Sym [−10S,10N], NCEP2 and NOAA 1997–2008

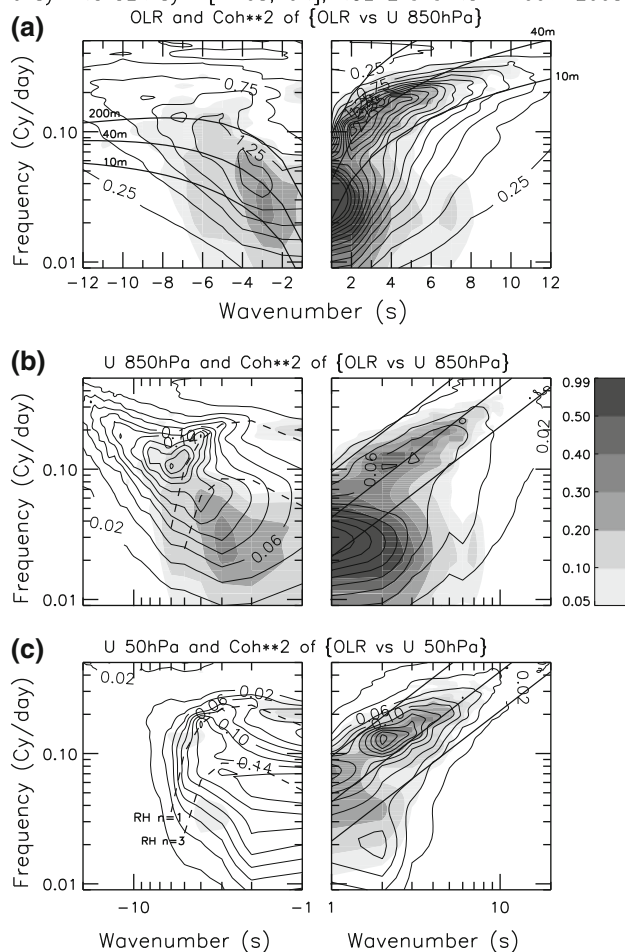


Fig. 8 Same as Fig. 7 but from the NCEP and NOAA data over the period 1997–2008. The number of doF is now around 450 for this value the 10, 5, and 1% level for the coherencies are at around 0.05, 0.1 and 0.3, respectively

times the spectra to be energy conserving. In the westward direction, the OLR spectrum has enhanced power along the dispersion curve of the equatorial Rossby waves in the model as in the observations. The coherency with the zonal wind at 850 hPa is also quite significant in the model although slightly smaller than in the observations, indicating that the model simulates the Rossby CCEWS.

In the eastward direction, the OLR spectra from the model has a relative maximum around $s = 3$ for periods above 16 days, well below the dispersion curve of Kelvin waves (Fig. 7a). The signature of the Kelvin waves on the OLR that is clearly apparent in the observations in Fig. 8a is almost absent from the model. Some coupling between Kelvin waves and OLR appear nevertheless on the coherency with the zonal wind at 850 hPa (dashed contours). Again, the signal is much less pronounced than in observations where the relative maximum in coherency matches the maximum in spectral amplitude for OLR. In the model

also, the enhanced coherency is limited to the highest wavenumbers $s = 1\text{--}4$ instead of extending up to the wavenumber $s = 10$.

Still in the eastward direction and close to $s = 1$, model and observations also has enhanced power for periods around 33–100 day ($0.01 < \omega < 0.3 - 0.4$) corresponding to the MJO. Again the spectral amplitude and coherencies are smaller in the model, consistent with our results about the MJO in Sect. 2.

3.1.2 Zonal wind spectra and coherency with OLR

The spectra for the zonal winds in Figs. 7b, c and 8b, c are displayed with both axis using a log-scale so the figures present the frequency times the wavenumber times the spectra to be again energy conserving. This display is well adapted to detect stratospheric waves in the equatorial regions: each maxima identified when one uses this display being associated without ambiguity with large-scale equatorially trapped waves or with Rossby Haurwitz waves (Lott et al. 2009).

In the model, and in the westward direction, the spectra for the zonal wind at 850 hPa in Fig. 7b resembles quite well that from NCEP in Fig. 8b. Although the coherency with OLR falls between the curves of the Rossby waves (see discussion before), it is noticeable that it is not this Rossby wave signal that dominates the spectra of the wind in the westward direction. The dominant periods and wavenumber are those of the Rossby-Haurwitz planetary waves (dashed lines). We attribute the relatively good performance of the model to represent this spectral signal, to the fact that our model represents well the midlatitudes low-frequency variability (see Lott et al. 2005). Interestingly, the fact that the Rossby Haurwitz waves do not appear in the OLR spectra in Figs. 7a and 8a, certainly follows that they are almost barotropic and correspond to very weak vertical velocities.

In the eastward direction, the zonal wind spectra in Fig. 7b is characterized by a relative maximum near between the dispersion curves of the Kelvin waves and that is strongly reminiscent with that in the observations in Fig. 7b. In the model nevertheless, this maxima does not coincide with an extrema in the coherency with OLR, as it does almost exactly in the observations. Although there seems to be tropospheric Kelvin waves in the model, their convectively coupled nature does not seem to be well captured.

Higher up at 50 hPa, the signal in the model is clearly dominated by the Rossby Haurwitz waves in the westward direction (Fig. 7c), as is also quite true for the NCEP data in Fig. 8c. This is consistent with the analysis in Lott et al. (2009) where the $s = 1$, $n = 1$ and 3 waves at periods around 5 and 16 days respectively were shown to affect substantially the tropics at this altitude.

Still at 50 hPa, but in the eastward direction, the MJO signature on the wind has almost entirely disappeared in the model (Fig. 7c), whereas in the observations in Fig. 8c it is quite significant, in agreement with the observational results in Weare (2010). For both the model and observations nevertheless, the spectra are largely dominated by Kelvin waves, those having periods slightly shorter than at 850 hPa. The Kelvin waves in the stratosphere are also related to convection, as indicate the significant values for the coherencies. In the model again, this relation is weaker than in the observations.

3.2 Kelvin waves composites

The fact that the observed Kelvin waves in the stratosphere appear quite close to the periods of the CCEWs suggests that a good simulation of the latter is a pre-requisite to have realistic stratospheric Kelvin waves. However, our model also produces realistic Kelvin waves in the stratosphere whereas it underestimates their convectively coupled nature in the troposphere, somehow contradicting what can be inferred from observations.

To clarify these points we next proceed as in Lott et al. (2009) and make a composite analysis. To extract the waves we apply to all fields a time-space band-pass filter which transfer function is applied as a multiplication in the Fourier space. The transfer function we chose is very broad since it keeps almost all the periods between 2.5 and 50 day for eastward wavenumbers between $s = 1$ and $s = 6$. Its transfer function in Fig. 9 largely includes the spectral domains of both the tropospheric and the stratospheric Kelvin waves. To diagnose when a Kelvin wave is present at 50 hPa, we then define an index which, at a given time, is the maximum value when the longitude varies of the filtered zonal wind averaged between 10°S and 10°N . We consider the zonal wind because the Kelvin waves are characterized by a strong signal on its equatorial

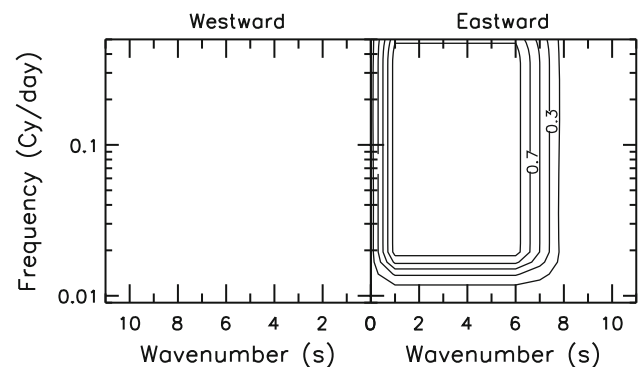


Fig. 9 Fourier transform of the transfer function of the filter used to extract the Kelvin waves in the analysis and observational datas (NCEP and NOAA OLR), and in the ipslcm5 model

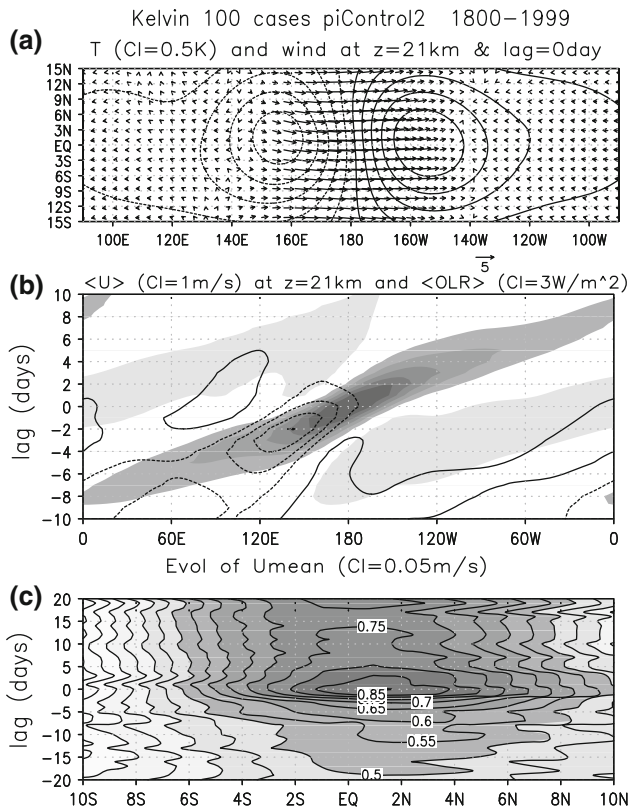


Fig. 10 Composite of the stratospheric Kelvin waves from picontrol2 and for the period 1800–2000, see text for details and subfigure titles for intervals. **a** Temperature and wind at 0d-lag; **b** Hovmöller plot of the OLR (line with negative values dashed) and of the zonal wind (light grey for negative values, strong grey for positive, values between ± 0.5 m/s are white); both OLR and wind are averaged over the equatorial band (10°S – 10°N); **c** Latitude versus time plot of the unfiltered zonal mean zonal wind, the contour interval for the shading is 0.1 m/s

average (Figs. 8c, 7c). Then the composites are built from dates selected when the index presents a maximum that exceeds a given threshold (see Lott et al. 2009). The selected threshold is chosen so that no more than one event every two years is selected.

The maps for the composite wind and temperature in Fig. 10a shows that our technique well captures the structure of the stratospheric Kelvin waves described in Lott et al. (2009), with wind anomalies at zero lag that are zonal and that are in quadrature with the temperature anomalies. When compared with the Kelvin waves packets in Fig. 4 from Lott et al. (2009) nevertheless, the structure on temperature also shows a substantial planetary wave $s = 1$ signature. This follows that the filter we have chosen is very broad (see Fig. 9) so the composite techniques combine the Kelvin wave packets and the planetary scale $s = 1$ Kelvin waves in a same signal. The wind composite in the model also resembles the wind composite from NCEP in Fig. 11a, and the temperature composite in the model is more pronounced. Also, the planetary scale $s = 1$

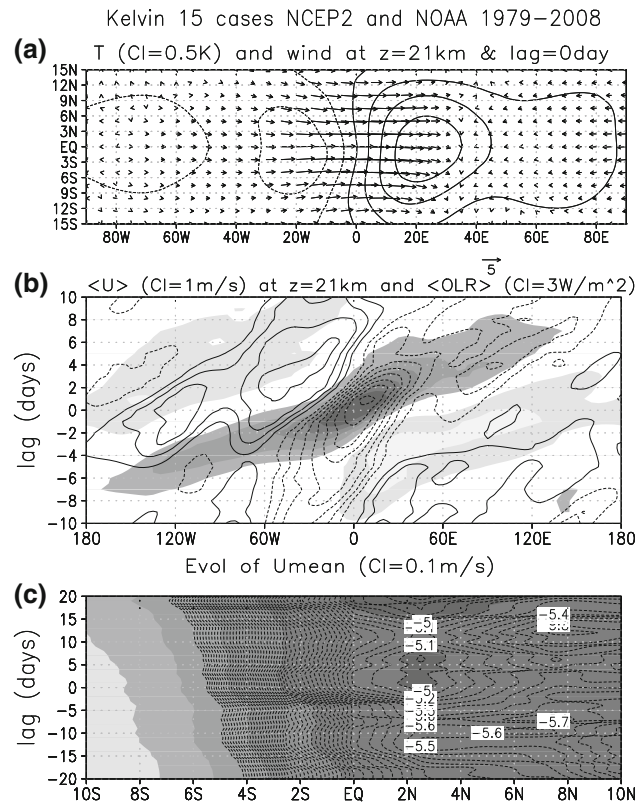


Fig. 11 Same as Fig. 10 but from the NCEP dataset and the NOAA OLR for the period 1979–2008. In **c** the contour interval for the shading is 2 m/s

contributes less to the temperature structure in the model than in NCEP. On top of being realistic on the amplitudes and shapes for the horizontal wind and Temperature, Fig. 10b shows that the temporal evolution of the Kelvin wave in the model stratosphere (illustrated by the evolution of the zonal wind at the Equator) is also realistic in duration and horizontal phase speed (a direct visual inspection gives $C \approx 20\text{m/s}$ in both).

As expected from the coherencies in Fig. 7c and Fig. 10b also shows that in the model, there is a substantial signal on OLR related to the Kelvin wave. The signal in OLR precedes that on the wind and both evolve on a comparable time scale. These two results tell that the convective signal is quite a direct forcing of the Kelvin waves in the model. Obviously this forcing is not the only one, as already indicated by the rather weak coherencies in Fig. 7c. When compared to the composites from the observations in Fig. 11b, the model signal on OLR is weaker, telling that the convective forcing of the stratospheric waves is less important in the model than in the observations.

It is also remarkable that in the model in Fig. 10b, the OLR signal evolves on a faster scale than in the observations in Fig. 11b. Also in the model, the OLR signal well precedes that on the wind whereas in the observations it

accompanies it (the observed OLR signal is even more pronounced after the time when the wind signal is the largest). Our interpretation of these results is that in the real world, the stratospheric waves occur predominantly during the life cycle of the tropospheric Kelvin CCEWS, as if the CCEWS were radiating waves toward the stratosphere. In the model on the other hand, where there are less CCEWS, this intimate relation between the CCEWS in the troposphere and the freely propagating ones in the stratosphere seems absent. In the model, the stratospheric wave response seems more like a dynamically filtered response to an unorganised forcing (this could explain the time lag between the stratospheric signal and the tropospheric ones). This interpretation, where the model lacks of an organized tropospheric forcing and replaces it in part by an unorganized one, would be more convincing if the Kelvin waves in the model stratosphere were less pronounced, which is not obvious when we look at direct fields like the temperature or the wind. As we shall see in the following, such an underestimation by the model appears more clearly when we look at the action of the waves on the mean flow.

3.3 Wave-mean flow interaction and relation with the ENSO

3.3.1 Mean flow composites

To illustrate the action of the waves on the mean flow, Fig. 10c shows composites of the zonal mean zonal wind during the life cycle of the waves. In it we see that the zonal wind increases by around 0.35 m/s between the lags $l = -20$ day and $l = 0$ day and decreases after. The accelerating phase between $l = -20$ day and $l = 0$ day is consistent with the fact that an upward propagating wave with positive phase velocity increases the mean zonal wind when its amplitude grows at a given altitude (see for instance Grimshaw 1975). During the decaying phase of the wave the zonal wind decays, again consistent with theory, but only return to its initial value if the waves is not dissipated. Here we see that the zonal mean zonal wind indeed decreases after the passage of the wave but return to a value which is around 0.25 m/s above its initial value: the Kelvin waves are partly dissipated. Note also that the 0.2 m/s changes that occur in around 5–10 days is quite small compared to the 0.1 m/s/day wave induced tendencies needed to drive the QBO variation in GCMs (see for instance Giorgetta et al. 2006 and Kawatani et al. 2010). It is also quite small compared with the tendency due to the $s = 1 - 6$ Kelvin waves and that was derived from satellite observations by Ern et al. (2008).

The same analysis done on the reanalysis field in Fig. 11c reveals two things. The first one is that the zonal mean zonal wind is predominantly negative, which

naturally follows that Kelvin waves propagate more easily during easterly phases of the QBO (our composite technique select almost automatically the eastward phases of the QBO when it detects large Kelvin waves, see also Yang et al. 2011). The second one is that the zonal mean wind slightly increases in the equatorial band, eventually consistent with the fact that Kelvin waves accelerate the zonal mean wind. Nevertheless, in the case of the reanalysis, it is impossible to attribute the zonal mean wind variations to the passage of the waves, since during westerly QBO phases the wind naturally evolves toward the easterly phase and this is not only due to the large scale Kelvin waves we extract from our composite. To be able to extract the action of the wave on the mean flow in the model, via the composite analysis, we clearly take advantage of the fact that our model does not simulate the QBO.

As the composite technique can not be used to compare the Kelvin waves acceleration between the model and the observations, the small acceleration detected in the model and compared to those documented elsewhere (Giorgetta et al. 2006; Ern and Preusse 2009), are our evidence that in the model the Kelvin waves are underestimated. The fact that the model Kelvin waves seem realistic on other fields, like the wind and temperature, follows that in the model the intrinsic frequency is smaller than in the observation (where the background wind is negative in the composite see Fig. 11c): for a same wave energy (roughly the amplitude as measured by winds and temperature) the vertical flux of action is larger for waves with larger intrinsic frequency: according to gravity waves theory this flux varies like the intrinsic frequency times the wave energy. Finally, we should recall here that such analysis should be extended to other waves, like the faster Kelvin waves, the Rossby gravity waves, and the inertio-gravity waves, and which also contribute to the QBO forcing.

3.3.2 ENSO and Kelvin waves

The fact that the Kelvin waves influence the zonal mean zonal flow, plus the fact that they are partly driven by the convection suggests that the intra-seasonal variations in convection related to the model ENSO for instance, can affect the stratospheric Kelvin waves amplitude. This issue is potentially significant since there is a growing number of evidences that the ENSO and the QBO oscillations are somehow related.

To address this issue we have conducted the above analyses of Kelvin waves distinguishing between the ENSO+ years from the ENSO- years that have been used to build Fig. 5. The spectra for OLR show significant differences at many periods and wavenumbers, and particularly at those corresponding to the stratospheric Kelvin waves (not shown). As a consequence, the spectra for the

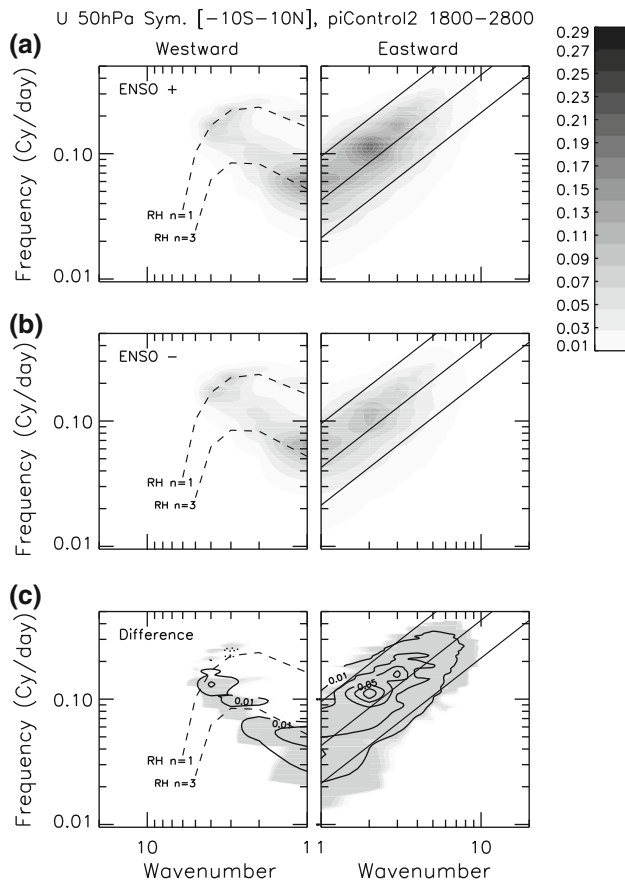


Fig. 12 Spectra of the zonal wind at 50 hPa in picontrol2 during model positive ENSO years (a), negative ENSO years (b) and differences (c). The differences in (c) are in solid and the confidence levels are shaded: the 5% and 1% confidence level are almost exactly superposed, they are derived assuming a normal distribution around the mean for each spectral peaks

zonal wind in the stratosphere are also significantly different with more Kelvin waves during ENSO+ years (Fig. 12). This result is confirmed when we build composite of Kelvin waves: for the same number of years in each ENSO phase and for the same threshold to detect Kelvin waves, we have more dates that enter in the composites during the positive ENSO phases than during the negative ones.

4 Discussion

In this paper the tropospheric equatorial variability of the pre-industrial 1,000-years long simulation done with the IPSLCM5 model has been analysed and compared with observations and re-analysis data covering the last 30-years. The use of datasets with such different length is necessary because in the model, some modes of variability like the intra-seasonal oscillation in Sect. 2 are

underestimated. An analysis of a shorter sample would have lead us to conclude that those modes are always absent, which is not quite true. The length of the model dataset was also used to analyse the inter-relation between some of these modes of variability, like the ENSO and the equatorial Kelvin waves, a task that is almost impossible to do with present days datasets because the different intra-seasonal oscillations that affect the tropics are very slow and have close periods. Finally, the use of long datasets also permit to quantify better second order processes that are nevertheless essential, like the wave-mean flow interactions that accompany the life cycle of an equatorial wave packets through the stratosphere (Sect. 3.3).

Our analysis of the inter-annual variability in Sect. 2 shows that the model has an ENSO-like oscillation, of about the right amplitude and time-scales. Nevertheless, the model ENSO is much too confined to the western Pacific. This defect is a known defect of some coupled models (for the CMIP3 models see Leloup et al. 2008). At the intra-seasonal time scales, the model also has problems in representing the MJO variability: only one typical event occurs in the model every 10–20 years typically, instead of 1–2 years in reality. This is consistent with Xavier et al. (2010), who have shown that this is a characteristic error of the models where the convection parameterization scheme is little based on the large scale moisture convergence.

Still in the troposphere and at shorter periods, the model simulates tropospheric Rossby and Kelvin CCEWs. In the model nevertheless, the “convectively coupled” nature of the Kelvin waves is in part lost: there is almost no Kelvin waves signature on the OLR spectra (left panels in Figs. 7a, 8a), and the coherency between the OLR and the tropospheric zonal wind is weaker than in observations. This tropospheric Kelvin waves signal is essentially apparent on the zonal wind Spectra at 850 hPa (right panel in Fig. 7b). This result is again quite consistent with the Straub et al. (2010)’s analysis of the CMIP3 database.

In the stratosphere, the IPSLCM5 model has about the right amount of Kelvin waves if we look at the 50 hPa zonal wind spectra (Figs. 7c, 8c), and this signal on the wind is also coherent with the OLR signal. Although this is consistent with the fact that convection in good part forces the stratospheric waves, the coherency is smaller than in the observations.

More qualitatively, the composite analyses in Sect. 3.2 shows that the relation between convection and the stratospheric waves is quite different between the observations and the model. In the observations, the composites of the OLR and of the zonal wind in the stratosphere are almost simultaneous (Fig. 11). The convective signal evolves over a substantially slower time scale (e.g., more the time scale of the CCEWs), and is also delayed compared to the stratospheric wind signal. As it is very unlikely

that the stratospheric Kelvin waves have an effect on the convection below, we attribute this last behaviour, and also the slower time scale of convection, to the fact that in reality the stratospheric Kelvin waves often accompany the development of the Kelvin CCEWs. In this case, the stratospheric signal associated with the CCEWs is faster than the tropospheric ones, which follows that the slowest waves belonging to CCEWs spectrum have shorter vertical wavelengths and are therefore more easily dissipated. In the model the development of the stratospheric Kelvin waves is following the tropospheric signal on OLR, consistent with the fact that convection in part forces the waves. It seems that in the model, the stratospheric waves signal that is due to convection, simply results from a dynamical filtering of all the waves excited by an almost disorganized convective signal. As the Kelvin wave signal on wind and Temperature has about the right amplitude, these result suggests that a good representation of the convectively coupled waves is not necessarily a pre-requisite to have about the right amount of stratospheric Kelvin waves in models.

The fact that the nature of the dominant relation between the convection and the stratospheric waves are quite different between the model and the observations, does not mean that the two behaviours are exclusive one from the other. Our composite analysis just tells that one behaviour dominates in the model whereas the other dominates in the observation. In the future, it could be interesting to analyse which dominates in the other models with stratosphere participating to CMIP5, and to extend this analysis to the other equatorial waves that penetrate into the stratosphere, like the Rossby-gravity waves. For the latter, it would be very instructive to consider the models that simulate a QBO, since the waves with negative phase speed penetrates better in the stratosphere when the zonal wind is positive.

On top of clarifying the relation between the stratospheric waves and the convection below, the composite analysis also permits to illustrate well the wave mean flow interaction which is at the basis of the QBO dynamics. In Fig. 10c we see that during the passage of a Kelvin wave packet the zonal mean zonal wind increases in the equatorial region before decreasing again. This behaviour is characteristic of the wave mean flow interaction occurring during the passage of a wave packet with positive phase speed. Note that the composite zonal wind does not return to its initial value after the passage of the wave, indicating that the Kelvin waves are partly dissipated in the model lower stratosphere. Note also that the accelerations seen in Fig. 10c are well below those needed to produce a tendency comparable to the QBO tendency. This is probably our better evidence here that the model does not simulate enough Kelvin waves, and may be that the weakness of the convective signal associated with the tropospheric Kelvin waves is causing this deficit.

Finally, our comprehensive analysis of the tropical variability, from the very slow-scales of ENSO to the synoptic scales of the equatorial waves, permit to analyse the relations between the two. As the equatorial waves force the QBO this can help clarifying the significance of the relations between the ENSO and the QBO oscillations suggested by various authors. As a first step in this direction, we have found that the ENSO signal has a substantial influence on the stratospheric Equatorial Kelvin wave signal (Fig. 12). Again this issue will need to be extended to models that simulate both a QBO and an ENSO, and to other type of waves.

References

- Anstey JA, Shepherd TG, Scinocca JF (2010) Influence of the Quasi-Biennial oscillation on the extratropical winter stratosphere in an atmospheric general circulation model and in reanalysis data. *J Atmos Sci* 67:1402–1419
- Baldwin MP, Gray LJ, Hamilton K, Haynes PH, Randel WJ, Holton JR, Alexander MJ, Hirota I, Horinouchi T, Jones DBA, Kinnerson JS, Marquardt C, Sato K, Takahashi M (2001) The Quasi-biennial oscillation. *Rev Geophys* 39:179–229
- Baldwin MP, Dunkerton TJ (1999) Downward propagation of the Arctic Oscillation from the stratosphere to the troposphere. *J Geophys Res* 104:30,937–30,946
- Barnett TP (1992) The interaction of multiple time scales in the tropical system. *J Clim* 4:269–285
- Bony S, Emanuel KA (2001) A parameterization of the cloudiness associated with cumulus convection; evaluation using TOGA COARE data. *J Atmos Sci* 58:3158–3183
- Boville BA, Randell WR (1992) Equatorial waves in a stratospheric GCM: effects of vertical resolution. *J Atmos Sci* 49:785–8001
- Cagnazzo C, Manzini E (2009) Impact of the stratosphere on the winter tropospheric teleconnections between ENSO and the North Atlantic and European Region. *J Clim* 22:1223–1238. doi:10.1175/2008JCLI2549.1
- Calvo N, Giorgetta MA, Garcia-Herrera R, Manzini E (2009) Nonlinearity of the combined warm ENSO and QBO effects on the Northern Hemisphere polar vortex in MAECHAM5 simulations. *J Geophys Res-Atmos* 114:D13109. doi:10.1029/2008JD011445
- Chiodi AM, Harrison DE (2010) Characterizing Warm-ENSO variability in the Equatorial Pacific: an OLR perspective. *J Clim* 23:2428–2439
- Christiansen B (2001) Downward propagation of zonal mean zonal wind anomalies from the stratosphere to the troposphere: model and reanalysis. *J Geophys Res* 106:27,307–27,322
- Douville H (2009) Stratospheric polar vortex influence on Northern Hemisphere winter climate variability. *Geophys Res Lett* 36:L18703. doi:10.1029/2009GL039334
- Dunkerton TJ (1997) The role of gravity waves in the quasi-biennial oscillation. *J Geophys Res* 102:26,053–26,076
- Dufresne JL et al. (2011) Overview of the IPSL-CM5 earth system model with an emphasis on model and forcing changes from CMIP3 to CMIP5. *Clim Dyn*. In preparation Climate Dynamics, this special issue
- Emanuel KA (1993) A cumulus representation based on the episodic mixing model: the importance of mixing and microphysics in predicting humidity. *AMS Meteorol Monogr* 24(46):185–192

- Ern M, Preusse P, Krebsbach M, Mlynczak MG, Russell JM (2008) Equatorial wave analysis from SABER and ECMWF temperatures. *Atmos Chem Phys* 8:845–869
- Ern M, Preusse P (2009) Quantification of the contribution of equatorial Kelvin Waves to the QBO wind reversal in the stratosphere. *Geophys Res Lett* 36:L21801. doi:[10.1029/2009GL040493](https://doi.org/10.1029/2009GL040493)
- Fraedrich K, Muller K (1992) Climate anomalies in Europe associated with ENSO extremes. *Int J Climatol* 1:25–31
- Giorgetta MA, Manzini E, Roeckner E, Esch M, Bengtson L (2006) Climatology and forcing of the quasi-biennial oscillation in the MAECHAM5 model. *J Clim* 19:3882–3901
- Goulet L, Duvel J-P (2000) A new approach to detect and characterize intermittent atmospheric oscillations: application to the intra-seasonal oscillation. *J Atmos Sci* 57:2397–2416
- Grimshaw R (1975) Nonlinear internal gravity waves and their interaction with the mean wind. *J Atmos Sci* 32:1779–1793
- Hamming RW (1983) Kaiser windows and optimization. *Digital Filters*, Prentice Hall, Englewood Cliffs, NJ, pp 185–207
- Hardiman SC, Butchart N, Haynes PH, Hare SHE (2007) A note on forced versus internal variability of the stratosphere. *Geophys Res Lett* 34:L12803. doi:[10.1029/2007GL029726](https://doi.org/10.1029/2007GL029726)
- Hardiman SC, Butchart SCN, Osprey SM, Gray LJ, Buschell AC, Hinton TJ (2010) The climatology of the middle atmosphere in a vertically extended version of the Met Office's climate model. Part I: mean state. *J Atmos Sci* 67:1509–1525
- Hendon HH, Wheeler MC (2008) Some space-time spectral analysis of tropical convection and planetary scale waves. *J Atmos Sci* 65:2936–2948
- Holton JR, Tan HC (1980) The influence of the equatorial quasi-biennial oscillation on the global circulation at 50mb. *J Atmos Sci* 37:2200–2208
- Horinouchi T, Pawson S, Shibata K, Manzini E, Giorgetta MA, Sassi F, Wilson RJ, Hamilton K, DeGrandpe J, Scaife AA (2003) Tropical cumulus convection and upward propagating waves in middle-atmospheric GCMs. *J Atmos Sci* 60:2765–2782
- Hourdin F, Musat I, Bony S, Braconnot P, Codron F, Dufresne J-L, Fairhead L, Filiberti M-A, Friedlingstein P, Grandpeix J-Y, Krinner G, Levan P, Lott F (2006) The LMDZ4 general circulation model: climate performance and sensitivity to parametrized physics with emphasis on tropical convection. *Clim Dyn* 27:787–813. doi:[10.1007/s00382-006-0158-0](https://doi.org/10.1007/s00382-006-0158-0)
- Hourdin F, Foujols M-A, Codron F, Guemas V, Dufresne J-L, Bony S, Denvil S, Guez L, Lott F, Ghattas J, Braconnot P, Marti O, Meurdesoif Y, Bopp L (2011) Climate and sensitivity of the IPSL-CM5A coupled model: impact of the LMDZ atmospheric grid configuration. Submitted to *Climate Dynamics*, this special issue
- Kawatani Y, Sato K, Dunkerton TD, Watanabe S, Miyahara S, Takahashi M (2010) The roles of the equatorial trapped waves and inertia-gravity waves in driving the Quasi-Biennial Oscillation. Part I: zonal mean wave forcing. *J Atmos Sci* 67:963–980
- Kessler WS (2001) EOF representation of the Madden-Julian oscillation and its connection with ENSO. *J Clim* 14:3055–3061
- Leloup J, Lengaigne M, Boulanger JP (2008) Twentieth century ENSO characteristics in the IPCC database. *Clim Dyn* 30:277–291
- Liebmann B, Smith CA (1996) Description of a complete (interpolated) outgoing longwave radiation dataset. *Bull Am Meteorol Soc* 77:1275–1277
- Lott F, Robertson AW, Ghil M (2004) Mountain torques and northern-hemisphere low-frequency variability. Part I: hemispheric aspects. *J Atmos Sci* 61:1259–1271
- Lott F, Fairhead L, Hourdin F, Levan P (2005) The stratospheric version of LMDz: dynamical climatologies, arctic oscillation, and impact on the surface climate. *Clim Dyn* 25:851–868. doi:[10.1007/s00382-005-0064-x](https://doi.org/10.1007/s00382-005-0064-x)
- Lott F, Kuttippurath J, Vial F (2009) A Climatology of the Gravest waves in the equatorial lower and middle stratosphere: method and comparison between the ERA-40 re-analysis and the LMDZ-GCM. *J Atmos Sci* 66:1327–1346
- Manzini E, Hamilton K (1993) Middle atmospheric traveling waves forced by latent and convective heating. *J Atmos Sci* 50:2180–2200
- Marti O, Braconnot P, Bellier J, Benshila R, Bony S, Brockmann P, Cadule P, Caubel A, Denvil S, Dufresne J-L, Fairhead L, Filiberti M-A, Foujols M-A, Fichet T, Friedlingstein P, Goosse H, Grandpeix J-Y, Hourdin F, Krinner G, Levy C, Madec G, Musat I, de Noblet N, Polcher J, Talandier C (2005) The new IPSL climate system model: IPSL-CM4. Notes du Pole de Modélisation de l'Institut Pierre Simon Laplace 26. ISSN 1288–1619
- Maruyama T, Tsunooka Y (1988) Anomalous short duration of the easterly wind phase of the qbo at 50 hpa in 1987 and its relationship to an el-NINO event. *J Meteor Soc Japan* 66:629–634
- Matthews AJ (2000) Propagation mechanisms for the Madden-Julian oscillation. *Q J R Meteorol Soc* 126:2637–2652
- Nikulin G, Lott F (2010) On the time-scales of the downward propagation and of the tropospheric planetary wave response to the stratospheric circulation. *Ann Geophys* 28:339–351
- Ricciardulli L, Garcia RR (2000) The excitation of equatorial waves by deep convection in the NCAR community climate model (CCM3). *J Atmos Sci* 57:3461–3487
- Sassi F, Kinnison D, Boville BA, Garcia RR, Roble R (2004) Effect of El Nino-Southern oscillation on the dynamical, thermal, and chemical structure of the middle atmosphere. *J Geophys Res-Atmos* 109:D17–D17108. doi:[10.1029/2003JD00443](https://doi.org/10.1029/2003JD00443)
- Salomon S, Rosenlof KH, Portmann RW, Daniel JS, Davis SM, Sanford TJ, GK (2010) Contributions of stratospheric water vapor to decadal changes in the rate of global warming. *Science* 327(5970):1219–1223
- Straub KH, Haertel PT, Kiladis GN (2010) An analysis of convectively coupled Kelvin waves in 20 WCRP CMIP3 global coupled climate models. *J Clim* 23:3031–3056
- Ropelewski CF, Jones PD (1987) An Extension of the Tahiti Darwin southern oscillation index. *Mon Weather Rev* 115:2161–2165
- Taguchi M (2010) Observed connection of the stratospheric quasi-biennial oscillation with El-Nino southern oscillation in radiosonde data. *J Geophys Res* 115:D18120. doi:[10.1029/2010JD014325](https://doi.org/10.1029/2010JD014325)
- Weare BC (2010) Madden Julian oscillation in the tropical stratosphere. *J Geophys Res* 115:D17113. doi:[10.1029/2009JD013748](https://doi.org/10.1029/2009JD013748)
- Wheeler MC, Hendon HH (2004) An all-season real-time multivariate MJO-index: development of an index for monitoring and prediction. *Mon Weather Rev* 132:1917–1932
- Wheeler M, Kiladis GN (1999) Convectively coupled equatorial waves: analysis of clouds and temperature in the wavenumber-frequency domain. *J Atmos Sci* 56:375–399
- Xavier PK, Duvel JP, Braconnot P, Doblas-Reyes FJ (2010) An evaluation metric for interannual variability and its application to CMIP3 twentieth-century simulations. *J Clim* 23:3497–3508
- Yang GY, Hoskins BJ, Slingo JM (2011) Equatorial waves in opposite QBO phases. *J Atmos Sci* 68:839–862